Received: 14 July 2020 | Revised: 3 September 2020 | Accepted: 14 September 2020

DOI: 10.1002/aoc.6040

Check for updates

FULL PAPER

Applied Organometallic Chemistry WILEY

Investigation of mononuclear, dinuclear, and trinuclear transition metal (II) complexes derived from an asymmetric Salamo-based ligand possessing three different coordination modes

Ruo-Nan Bian[1] | **Ji-Fa Wang**[1] | **Xin Xu**[1] | **Xiu-Yan Dong**[1] | **Yu-Jie Ding**[2]

[1]School of Chemical and Biological Engineering, Lanzhou Jiaotong University, Lanzhou, Gansu, 730070, China

[2]College of Biochemical Engineering, Anhui Polytechnic University, Wuhu, 241000, China

Correspondence
Xiu-Yan Dong, School of Chemical and Biological Engineering, Lanzhou Jiaotong University, Lanzhou 730070, China.
Email: dongxy@mail.lzjtu.cn

Yu-Jie Ding, College of Biochemical Engineering, Anhui Polytechnic University, Wuhu, 241000, China.
Email: dyj@ahpu.edu.cn

Funding information
Science and Technology Program of Gansu Province, Grant/Award Number: 18YF1GA057; Program for Excellent Team of Scientific Research in Lanzhou Jiaotong University, Grant/Award Number: 201706; National Natural Science Foundation of China, Grant/Award Number: 21761018

A new asymmetric Salamo-based ligand H_2L was synthesized using 3-*tert-butyl*-salicylaldehyde and 6-methoxy-2-[*O*-(1-ethyloxyamide)]-oxime-1-phenol. By adjusting the ratio of the ligand H_2L and Cu (II), Co (II), and Ni (II) ions, mononuclear, dinuclear, and trinuclear transition metal (II) complexes, [Cu(L)], [{Co(L)}$_2$], and [{Ni(L)(CH_3COO)(CH_3CH_2OH)}$_2$Ni] with the ligand H_2L possessing completely different coordination modes were obtained, respectively. The optical spectra of ligand H_2L and its Cu (II), Co (II) and Ni (II) complexes were investigated. The Cu (II) complex is a mononuclear structure, and the Cu (II) atom is tetracoordinated to form a planar quadrilateral structure. The Co (II) complex is dinuclear, and the two Co (II) atoms are pentacoordinated and have coordination geometries of distorted triangular bipyramid. The Ni (II) complex is a trinuclear structure, and the terminal and central Ni (II) atoms are all hexacoordinated, forming distorted octahedral geometries. Furthermore, optical properties including UV–Vis, IR, and fluorescence of the Cu (II), Co (II), and Ni (II) complexes were investigated. Finally, the antibacterial activities of the Cu (II), Co (II), and Ni (II) complexes were explored. According to the experimental results, the inhibitory effect was found to be enhanced with increasing concentrations of the Cu (II), Co (II), and Ni (II) complexes.

KEYWORDS
antibacterial activity, DFT, crystal structure, fluorescence property, Salamo-based ligand

1 | INTRODUCTION

The compound formed by the condensation of an aldehyde and amine is generally known as Schiff base, whereas the N_2O_2-donor chelated Schiff base (N,N′-disalicylideneethylenediamine, Salen) formed by the condensation of two identical aldehyde molecules and one diamine molecule is abbreviated as Salen.[1–5] Salen-based compounds have four coordination atoms (O, N, N, and O) in the center and can be coordinated with various metal ions to form M-Salen complexes.[6–8] The structure of N and O coordination with metal ions of Salen complexes,[9–12] which is close to the biological environment,[13–16] has attracted considerable attention in the field of molecular recognition.[17,18] In addition, M-Salen complexes have been widely used in various catalytic reactions due to their important and interesting structures,[19–22]

 © 2020 John Wiley & Sons, Ltd.

variable, simple synthesis route, and easy recycling of catalysts.[23,24]

After modification of Salen-based compounds, two more electronegative oxygen atoms were introduced into the Schiff base nitrogen atoms to form Salamo-based compounds.[25–32] In this paper, an asymmetric Salamo-based ligand H_2L was synthesized first, and the single crystals of the Cu (II), Co (II), and Ni (II) complexes were cultured successfully. For the ligand H_2L, this was a new Salamo-based compound synthesized for the first time. The reasons for the different crystal structures of the Cu (II), Co (II), and Ni (II) complexes were investigated. The Cu (II) complex had a 1:1 configuration, and the Cu (II) atom was only coordinated with the N_2O_2 cavity of the fully deprotonated ligand $(L)^{2-}$ unit. However, for the Co (II) complex, Co (II) atoms were coordinated not only with the N_2O_2 cavities of the ligand $(L)^{2-}$ units but also with bridging phenoxy oxygen atoms of another ligand $(L)^{2-}$ unit, which was the main reason for the different configuration from the Cu (II) complex. Intriguingly, the Ni (II) atoms were coordinated not only with the N_2O_2 cavities of the ligand $(L)^{2-}$ units but also with the oxygen atoms from the methoxy substituents of the ligand $(L)^{2-}$ unit, two ethanol molecules, and two acetate groups. The two bridging acetate groups, two bridging phenolic oxygen atoms, and two methoxy oxygen atoms connected together, the three Ni (II) atoms resulted in a 2:3 ($(L)^{2-}$: Ni (II)) configuration.

2 | EXPERIMENTAL

2.1 | Materials and general methods

All chemicals were purchased from Alfa Aesar and used without further purification. The organic solvents used in other experiments are analytical grade solvents and are commercially available from Tianjin Chemical Reagent Factory. Elemental (C, H, and N) analyses were performed on a GmbH Variuo EL V3.00 automatic elemental analyzer (Elementar, Berlin, Germany). The elements Cu (II), Co (II), and Ni (II) were analyzed by IRIS ER/S-WP-1 ICP atomic emission spectrometry. The melting points were obtained by using a microscopic melting point apparatus manufactured by Shanghai Instrument Physical Optical Instrument Company and were uncorrected. UV–vis absorption spectra were determined using a Shimadzu UV-3900 spectrometer (Shimadzu, Japan). Fluorescence spectra were performed on a Sanco 970-CRT fluorescence spectrophotometer equipped with a quartz cuvette having a path length of 1 cm, with the xenon lamp as an excitation source. IR spectra were recorded with a VERTEX70 FT-IR spectrophotometer (Bruker, Billerica, MA, USA), with samples prepared as KBr (500–4,000 cm^{-1}) and CsI (100–500 cm^{-1}) pellets. The X-ray crystal structures were determined by a SuperNova Dual Cu at zero AtlasS2 four-circle diffractometer. ESI-MS spectra was measured on the Bruker Daltonics Esquire 6000 mass spectrometer.

2.2 | X-ray crystallographic analysis

Crystal data of the Cu (II), Co (II), and Ni (II) complexes were gleaned on a SuperNova Dual Cu at zero AtlasS2 four-circle diffractometer with a monochromatic Mo-Ka radiation (λ = 0.71073 Å) source at 297, 100.01, and 297 K, respectively.

The single crystal structures were solved using direct methods (SHELXL).[33] Empirical absorption correction using spherical harmonics was implemented in SCALE3 ABSPACK scaling algorithm. Hydrogen atoms were included at the calculated positions and constrained to ride on their parent atoms. All nonhydrogen atoms were anisotropically refined.[34] The crystallographic data collection and refining of the Cu (II), Co (II), and Ni (II) complexes are listed in Table 1.

2.3 | The synthesis of the ligand H_2L

The synthetic route to H_2L is shown in Scheme 1.

2.3.1 | The synthesis of 3-*tert-butyl*-5-bromosalicylaldehyde

According to Guo et al,[35] 3-*tert-butyl*-salicylaldehyde (178.23 mg, 1.0 mmol) was dissolved in two-neck round bottom flask containing 20 ml of dichloromethane and 1.5 ml of liquid bromine, was drawn with a syringe, and injected into a constant pressure drop funnel containing 15 ml of dichloromethane. Keep the system sealed to a temperature of 0°C. Slowly add the brominated dichloromethane solution to the round bottom flask, and keep the temperature constant and react 1.5 h. After, anhydrous sodium sulfite solution (20 ml) was poured into the reactor and continued 0.5 h. Stop the reaction, the liquid was separated with a separating funnel, leaving the organic phase. It is then distilled under reduced pressure to give a bright yellow solid, namely, 3-*tert-butyl*-5-bromosalicylaldehyde, yield: 91.8% (236.05 mg). m.p.: 62°C–64°C. ^{1}H NMR spectrum of 3-*tert-butyl*-5-bromosalicylaldehyde as shown Figure S1. Anal. calcd. for $C_{11}H_{13}O_2Br$: C, 51.38; H, 5.10. Found: C,

TABLE 1 Crystal data and the structure refinements for the Cu (II), Co (II), and Ni (II) complexes

Complex	The Cu (II) complex	The Co (II) complex	The Ni (II) complex
Empirical formula	$C_{21}H_{23}BrCuN_2O_5$	$C_{42}H_{46}Br_2Co_2N_4O_{10}$	$C_{50}H_{64}Br_2N_4Ni_3O_{16}$
Formula weight	526.86	1044.51	1313.00
T (K)	297	100.01(10)	297.0
Wavelength (Å)	0.71073	0.71073	0.71073
Crystal system	triclinic	monoclinic	monoclinic
Space group	P-1	$P2_1/n$	$P2_1/c$
a (Å)	9.0707(17)	14.1050(7)	11.4285(7)
b (Å)	9.9746(9)	14.0806(9)	18.6781(15)
c (Å)	12.5380(13)	22.9478(17)	27.9719(17)
α (°)	79.100(8)	90	90
β (°)	89.171(12)	104.478(6)	95.070(6)
γ (°)	75.060(13)	90	90
V (Å^3)	1075.6(3)	4412.9(5)	5947.6(7)
Z	2	4	4
D_{calc} (g cm^{-3})	1.627	1.572	1.466
Absorption coefficient (mm^{-1})	2.908	2.623	2.349
F (000)	534.0	2120.0	2696.0
Crystal size (mm)	0.13 × 0.11 × 0.1	0.12 × 0.11 × 0.09	0.12 × 0.11 × 0.1
θ Range (°)	4.306–50	4.354–50	4.19–50
Index ranges	−7 ≤ h ≤ 10	−14 ≤ *h* ≤ 19	−13 ≤ h ≤ 11
	−11 ≤ k ≤ 11	−19 ≤ k ≤ 13	−20 ≤ k ≤ 22
	−14 ≤ l ≤ 14	−29 ≤ l ≤ 24	−32 ≤ l ≤ 33
Reflections collected/unique	7572/3774 [R_{int} = 0.0538]	23,053/10464 [R_{int} = 0.593]	27,675/10430 [R_{int} = 0.0566]
Completeness	99.7%	84.3%	99.6%
Data/restraints/parameters	3,774/9/275	10,464/0/549	10,430/51/704
GOF	1.089	1.024	1.022
Final R_1, wR_2 indices	0.0647, 0.1468	0.0631, 0.0934	0.0662, 0.1362
R_1, wR_2 indices (all data)	0.939, 0.1832	0.1175, 0.1113	0.1268, 0.1643
Largest diff. peak and hole (e.Å^{-3})	1.69/−0.62	0.70/−0.90	1.14/−0.48

50.51; H, 5.02. ^{1}H NMR (500 MHz, DMSO) *δ* 11.75 (s, 1*H*, –CHO), 9.96 (s, 1*H*, –OH), 7.89 (d, *J* = 2.5 Hz, 1*H*, –ArH), 7.57 (d, *J* = 2.5 Hz, 1*H*, –ArH), 1.37 (s, 9*H*, –CH3).

2.3.2 | The synthesis of 6-methoxy-2-[*O*-(1-ethyloxyamide)]-oxime-1-phenol

6-Methoxy-2-[*O*-(1-ethyloxyamide)]-oxime-1-phenol was prepared according to a previously reported method.[2,36] Weighing 1,2-bis (aminooxy)ethane 414.45 mg (4.5 mmol) in ethanol (20 ml), another 684.67 mg (4.5 mmol) of 3-methoxysalicylaldehyde was dissolved in ethanol (20 ml). An ethanol solution of 3-methoxysalicylaldehyde was added drop by drop to an ethanol solution of 1,2-bis (aminooxy)ethane in a water bath at 55°C, with a controlled drop acceleration of about 10 s a drop and continuous reaction for 6 h to obtain light yellow ethanol solution. Decompression distillation removes excess solvent and concentrates the reaction solution to about 5 ml. The concentrated solution is a bright yellow oily liquid, further purified by column chromatography to obtain white solid 748.44 mg, yield: 73.51%; m.p.: 95.5°C–96.5°C. Anal. Calcd. for $C_{10}H_{14}N_2O_4$: C, 53.09; H, 6.24; N, 12.38. Found: C, 53.32; H, 6.20; N, 12.16. ^{1}H NMR (500 MHz, $CDCl_3$) *δ* 3.92 (s, 3*H*), 3.96 (t, *J* = 4.5 Hz, 2*H*), 4.38 (t, *J* = 4.5 Hz, 2*H*), 5.50 (brs, 2*H*), 6.82 (dd, *J* = 7.8, 1.6 Hz, 1*H*), 6.87 (t, *J* = 7.8 Hz, 1*H*), 6.90 (dd, *J* = 7.8, 1.6 Hz, 1*H*), 8.24 (s, 1*H*), 9.88 (s, 1*H*).

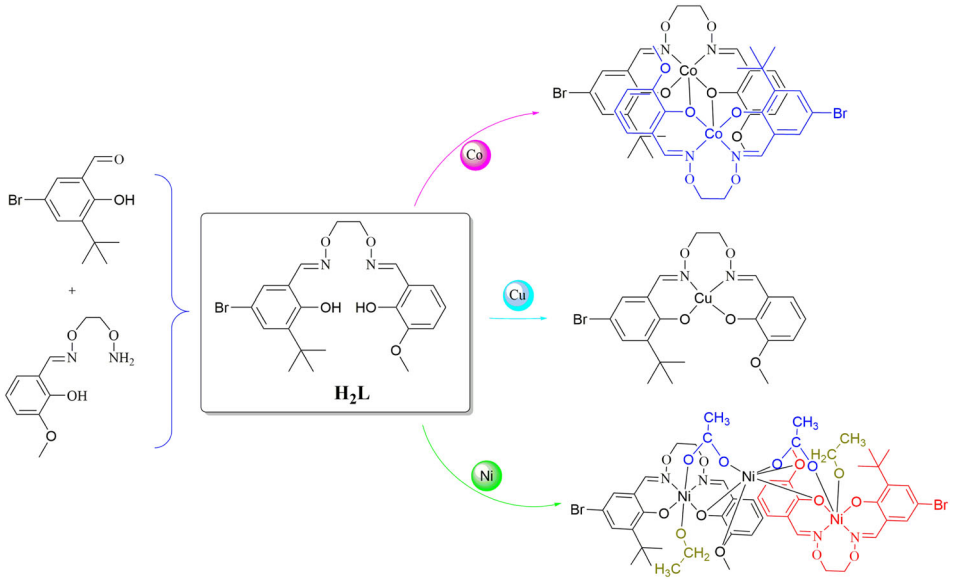

SCHEME 1 Synthetic route to H_2L and its Cu (II), Co (II), and Ni (II) complexes

2.3.3 | The synthesis of H_2L

A total of 257.13 mg (1 mmol) of 3-*tert-butyl*-5-bromosalicylaldehyde and 226.23 mg (1 mmol) of 6-methoxy-2-[*O*-(1-ethyloxyamide)]-oxime-1-phenol were respectively dissolved in 20 ml of absolute ethanol at room temperature and then reacted in a water bath at 60°C for 6 h by one pot method. After the reaction was completed, a pale yellow solution was obtained, and all excess solvent was removed by vacuum distillation to obtain a yellow viscous liquid (367.7 mg), yield: 79.02%; ^{1}H NMR spectrum of the ligand H_2L as shown Figure S2. Anal. Calcd. for $C_{21}H_{25}BrN_2O_5$: C, 54.20; H, 5.42; N, 6.02. Found: C, 54.67; H, 5.24; N, 5.92. ^{1}H NMR (500 MHz, $CDCl_3$) δ 10.32 (s, 1*H*), 9.72 (s, 1*H*), 8.26 (s, 1*H*), 8.15 (s, 1*H*), 7.35 (*d*, J = 2.3 Hz, 1*H*), 7.13 (*d*, J = 2.4 Hz, 1*H*), 6.92 (d, J = 7.9 Hz, 1*H*), 6.85(t, J = 7.8 Hz, 1*H*), 6.80(dd, J = 7.8, 1.5 Hz, 1*H*), 4.49 (s, 4*H*), 3.91 (s, 3*H*), 1.39 (s, 9*H*).

The ligand structure in DMF solution was confirmed by ESI-MS spectrum (m/z = 465.1406; Figure S3).

2.4 | Syntheses of the Cu (II), Co (II), and Ni (II) complexes

The synthetic route to the Cu (II), Co (II), and Ni (II) complexes is shown in Scheme 1.

The syntheses of the Cu (II), Co (II), and Ni (II) complexes are similar, so take the Cu (II) complex as an example to elaborate the syntheses of the three complexes. Synthesis of the Cu (II) complex: first, the ligand H_2L (4.65 mg, 0.01 mmol) was weighed and dissolved in ethyl acetate (EA) solvent (2 ml), and the color after dissolution was light yellow. Then weigh Cu $(OAc)_2{\cdot}H_2O$ (2.0 mg, 0.01 mmol) and dissolve it in 4 ml of ethanol solution. The solution is light blue and transparent. Then, the absolute ethanol solution of copper (II) acetate was added to the EA solution of the ligand, and the color of the solution turned dark brown immediately after the two solution was mixed. Stirred at room temperature for 30 min to fully react the ligand H_2L with copper (II) acetate. Finally, use cotton wool to filter the reacted solution into a vial in a funnel. Seal the bottle mouth with tin foil, and let it stand in a quiet and dark place. After 2 weeks of natural volatilization, black block crystals can be obtained for X-ray crystallographic analysis. Elemental analysis: Anal. calc. For [Cu(L)] ($C_{21}H_{23}BrCuN_2O_5$) (%): C, 47.87; H, 4.40; N, 5.32; Cu, 12.06. Found (%): C, 48.16; H, 4.35; N, 5.24; Cu, 12.13.

Elemental analysis: Anal. calc. For [{Co(L)}$_2$] ($C_{42}H_{46}Br_2Co_2N_4O_{10}$) (%): C, 48.30; H, 4.44; N, 5.36; Co, 11.28. Found (%): C, 48.51; H, 4.36; N, 5.19; Co, 11.30.

Elemental analysis: Anal. calc. For [{Ni(L)(CH_3COO)(CH_3CH_2OH)}$_2$Ni] ($C_{50}H_{62}Br_2Ni_3N_4O_{16}$) (%): C, 45.81; H, 4.77; N, 4.27; Ni, 13.43. Found (%): C, 46.11; H, 4.68; N, 4.18; Ni, 13.52.

2.5 | Experimental methods for inhibition rings

The experimental strains were *Escherichia coli* and *Staphylococcus aureus*; both of which are pathogenic bacteria, and their structure and biochemical characteristics have been completely studied and widely distributed.[37,38] The frozen strains were scribed, inoculated into plate medium, and cultured at 37°C for 24 h. The single colonies were inoculated into 100-ml liquid

medium, cultured at 37°C, 200 r/min overnight on shaking bed, and the bacterial liquid was reserved. The concentrations of H_2L samples were 0.5, 1.0, and 2.0 mg/ml for antimicrobial experiments.

3 | RESULTS AND DISCUSSION

A series of characterizations of the Cu (II), Co (II), and Ni (II) complexes were performed, including UV–Vis, IR, and fluorescence. Moreover, X-ray crystallographic analyses were also done. Finally, the structures of the Cu (II), Co (II), and Ni (II) complexes were determined, and the configurations of the central metal atoms of the complexes and the intramolecular and intermolecular hydrogen bondings are depicted.

3.1 | IR spectra

The IR spectra of the Cu (II), Co (II), and Ni (II) complexes are shown in Figure 1. For the ligand H_2L, the $\nu_{O\text{-}H}$ band was observed at approximately 3,414 cm^{-1}.[39,40] This band is disappeared in the IR spectra of the Cu (II), Co (II), and Ni (II) complexes, which is indicative of the fact that the phenolic OH groups of H_2L have been deprotonized and coordinated to the M (II) atoms.[13] Besides, in the spectra of the Cu (II), Co (II), and Ni (II) complexes, the $\nu_{O\text{-}H}$ bands of water molecules were found at approximately 3,436, 3,437, and 3,459 cm^{-1}, respectively. The δH_2O bands at approximately 1,600 cm^{-1} were covered by the strong C═N stretching bands. These bands of water molecules in the Cu (II), Co (II), and Ni (II) complexes were due to the introduction of KBr pressing plates. In addition, a strong C═N stretching vibration band was observed at approximately 1,615 cm^{-1}.[41–43] in the ligand H_2L, however, the C═N stretching vibration bands were found at approximately 1,598, 1,602, and 1,603 cm^{-1} in the Cu (II), Co (II), and Ni (II) complexes, respectively. The C═N stretching vibration bands of the Cu (II), Co (II), and Ni (II) complexes shifted to more lower wavenumbers, indicating that the metal (II) ions have coordinated with the oxime nitrogen atoms.[44] Next, a C–O stretching vibration band was observed at approximately 1,256 cm^{-1} in the ligand H_2L.[45,46] But C–O stretching vibration bands were observed at approximately 1,173, 1,215, and 1,217 cm^{-1} in the Cu (II), Co (II), and Ni (II) complexes, respectively. Compared with the C–O stretching vibration band of the ligand H_2L, the C–O stretching vibration bands of the Cu (II), Co (II), and Ni (II) complexes shifted to lower wavenumbers, indicating that the metal (II) ions have coordinated with the phenol oxygen atoms.[47,48] In addition, the characteristic bands of M–O were observed at approximately 419, 418, and 419 cm^{-1} in the Cu (II), Co (II), and Ni (II) complexes, respectively, and the characteristic bands of M–N were observed at approximately 542, 560, and 479 cm^{-1} in the Cu (II), Co (II), and Ni (II) complexes, respectively.[10,14,25,26] The above results are consistent with the results of elemental analyses and X-ray crystallographic analyses.

3.2 | UV–vis absorption spectra

The UV–Vis absorption spectra of the free ligand H_2L and its Cu (II), Co (II), and Ni (II) complexes in DMF are shown in Figure 2. From the UV–Vis absorption

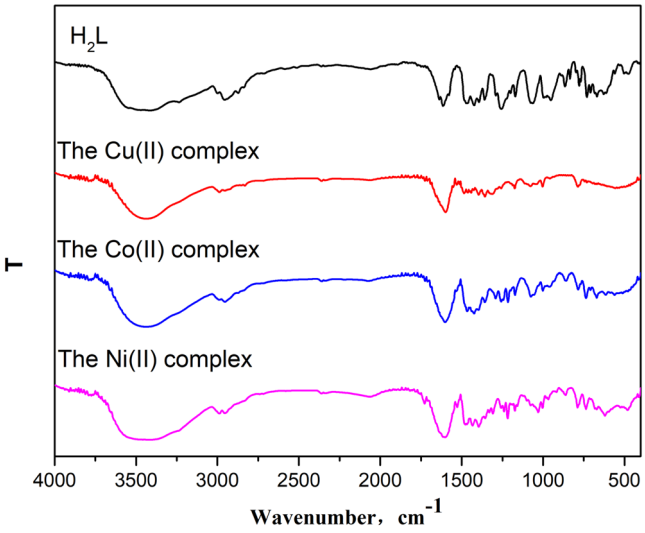

FIGURE 1 The IR spectra of H_2L and its Cu (II), Co (II), and Ni (II) complexes

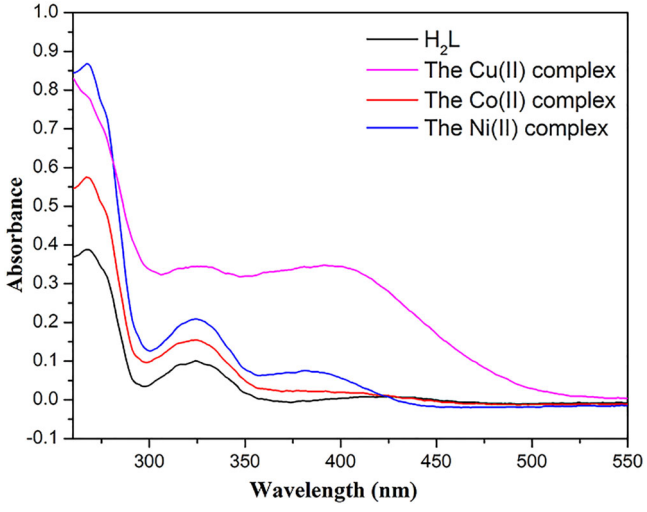

FIGURE 2 UV–vis spectra of H_2L and its Cu (II), Co (II), and Ni (II) complexes

TABLE 2 The selected bond lengths (Å) and angles (°) of the Cu (II), Co (II), and Ni (II) complexes

The Cu (II) complex			
Bond	**Lengths**	**Bond**	**Lengths**
Cu1–O1	1.890(6)	Cu1–N1	1.971(8)
Cu1–O2	1.896(7)	Cu1–N2	1.953(7)
Bond	**Angles**	**Bond**	**Angles**
O1–Cu1–O2	87.9 (3)	O1–Cu1–N1	89.3(3)
O1–Cu1–N2	159.6(3)	O2–Cu1–N1	153.8(3)
O2–Cu1–N2	91.0(3)	N1–Cu1–N2	100.3(3)
The Co (II) complex			
Bond	**Lengths**	**Bond**	**Lengths**
Co1–N1	2.035(3)	Co1–N2	2.103(4)
Co2–N3	2.019(3)	Co2–N4	2.089(4)
Co1–O1	1.924(3)	Co1–O4	2.083(3)
Co1–O9	1.987(3)	Co2–O4	1.975(3)
Co2–O6	1.905(3)	Co2–O9	2.082(3)
Bond	**Angles**	**Bond**	**Angles**
O6–Co2–O9	95.99(11)	O6–Co2–O4	119.57(12)
O6–Co2–N3	90.83(13)	O6–Co2–N4	105.59(13)
O9–Co2–N4	80.16(12)	O4–Co2–O9	76.32(11)
O4–Co2–N3	107.25(13)	O4–Co2–N4	130.54(12)
N3–Co2–O9	169.42(13)	N3–Co2–N4	90.24(14)
O9–Co1–O4	76.06(11)	O9–Co1–N1	102.93(13)
O9–Co1–N2	124.13(12)	O1–Co1–O9	123.11(12)
O1–Co1–O4	99.93(11)	O1–Co1–N1	90.11(13)
O1–Co1–N2	110.34(13)	O4–Co1–N2	80.26(12)
N1–Co1–O4	168.65(13)	N1–Co1–N2	91.33(14)
The Ni (II) complex			
Bond	**Lengths**	**Bond**	**Lengths**
Ni1–O1	2.030(4)	Ni1–O2	1.984(4)
Ni1–O9	2.064(4)	Ni1–O10	2.111(4)
Ni1–N2	2.079(5)	Ni1–N3	2.023(6)
Ni2–O4	1.998(4)	Ni2–O7	2.065(4)
Ni2–O12	1.999(4)	Ni2–N1	2.020(5)
Ni2–O15	2.124(5)	Ni2–N4	2.061(6)
Ni3–O1	1.991(3)	Ni3–O3	2.014(4)
Ni3–O5	2.157(4)	Ni3–O11	2.158(5)
Ni3–O12	1.986(4)	Ni3–O16	2.002(5)
Bond	**Angles**	**Bond**	**Angles**
O1–Ni1–O9	88.04 (17)	O1– Ni1–O10	91.65(17)
O1–Ni1–N2	84.78(18)	O2–Ni1–O1	89.08(16)
O2–Ni1–O9	174.39(16)	O2–Ni1–O10	86.83(18)
O2–Ni1–N2	91.17(18)	O2–Ni1–N3	86.22(19)
O9–Ni1–O10	88.44(18)	O9–Ni1–N2	93.36(18)

TABLE 2 (Continued)

Bond	Angles	Bond	Angles
N2–Ni1–O10	175.9(2)	N3–Ni1–O1	174.27(18)
N3–Ni1–O9	96.9(2)	N3–Ni1–O10	91.4(2)
N3–Ni1–N2	92.0(2)	O4–Ni2–O7	175.04(17)
O4–Ni2–O12	90.03(17)	O4–Ni2–N1	85.76(18)
O4–Ni2–O15	87.33(19)	O4–Ni2–N4	90.1(2)
O7–Ni2–O15	88.30(18)	O12–Ni2–O7	87.89(17)
O12–Ni2–N1	175.59(19)	O12–Ni2–O15	93.2(2)
O12–Ni2–N4	84.8(2)	N1–Ni2–O7	96.41(18)
N1–Ni2–O15	87.9(2)	N1–Ni2–N4	93.9(2)
N4–Ni2–O7	94.1(2)	N4–Ni2–O15	176.8(2)
O1–Ni3–O3	97.73(16)	O1–Ni3–O5	76.87(15)
O1–Ni3–O11	88.38(16)	O1–Ni3–O16	94.96(18)
O3–Ni3–O5	90.05(18)	O3–Ni3–O11	171.91(19)
O5–Ni3–O11	86.17(19)	O12–Ni3–O1	160.6(2)
O12–Ni3–O3	96.10(18)	O12–Ni3–O5	89.66(18)
O12–Ni3–O11	76.75(18)	O12–Ni3–O16	97.7(2)
O16–Ni3–O3	93.1(2)	O16–Ni3–O5	171.58(16)
O16–Ni3–O11	91.6(2)		

spectra, it can be observed that the free ligand H_2L has two absorption peaks, with wavelengths at about 267 and 322 nm, respectively. The absorption peak at 267 nm belongs to the $\pi - \pi^*$ transition in the benzene rings, whereas the peak at 322 nm is assigned to the $\pi - \pi^*$ transition of oxime groups.[49] However, there were two sets of peaks in the Cu (II) complex. The absorption peak of the $\pi - \pi^*$ transition of the benzene ring in the Cu (II) complex is weakened or disappeared due to the fine structure of the benzene ring that is slightly altered by the coordination of the metal.[15] The peak at 267 nm in H_2L was disappeared in the Cu (II) complex, indicating that the Cu (II) atom has coordinated with H_2L.[50] A new absorption peak at about 398 nm was caused by LMCT. There were three absorption peaks in the UV–Vis absorption spectrum of the Co (II) complex. The first two peaks were consistent with the ligand H_2L, but the Co (II) complex had a new absorption peak at about 405 nm. The appearance of new absorption peak should be appointed to the LMCT of ligand–metal coordination.[51] There were three sets of absorption peaks in the Ni (II) complex, at about 267, 322, and 383 nm, respectively. The new absorption peak at 383 nm was attributed to the coordination between the Ni (II) atoms and the ligand, which was caused by LMCT.[52]

3.3 | Crystal structure descriptions

The structures of the Cu (II), Co (II), and Ni (II) complexes were determined by X-ray crystallographic analysis. The bond lengths and angles of the Cu (II), Co (II), and Ni (II) complexes are listed in Table 2. The hydrogen bonding interactions are listed in Table 3.

3.3.1 | Crystal structure of the Cu (II) complex

The crystal structure and coordination configuration of the Cu (II) complex are shown in Figure 3. The Cu (II) complex was formed by the completely deprotonized ligand $(L)^{2-}$ unit and one Cu (II) atom. The Cu (II) complex belongs to triclinic system with space group *P*-1.

The Cu (II) complex had a mononuclear ($(L)^{2-}$:Cu (II) = 1:1) structure. The Cu (II) atom was coordinated with two N atoms (N1, N2) and two O atoms (O1, O2) in the N_2O_2 cavity of the ligand $(L)^{2-}$ unit, forming a planar quadrilateral geometry.

In the $(L)^{2-}$ part, the H atom on the *tert-butyl* group forms intramolecular hydrogen bonds with the protonated phenoxy atom at the adjacent site, which

TABLE 3 Hydrogen bonding distances (Å) and bond angles (°) for the Cu (II), Co (II), and Ni (II) complexes

The Cu (II) complex				
D−H···A	d(D−H)	d(H···A)	d(D···A)	∠D−H···A
C11−H11A···O1	0.96	2.40	3.041(14)	124
C17−H17C···O1	0.96	2.31	2.963(14)	124
The Co (II) complex				
D−H···A	d(D−H)	d(H···A)	d(D···A)	∠ D−H···A
C8−H8C···O1	0.96	2.33	2.950(5)	122
C9−H9A···O1	0.96	2.39	3.031(5)	124
C21−H21B···O7	0.96	2.56	3.387(5)	145
C29−H29C···O6	0.96	2.37	3.012(5)	124
C30−H30A···O6	0.96	2.35	2.949(5)	120
C42−H42C···O2	0.96	2.55	3.256(5)	130
The Ni (II) complex				
D−H···A	d(D−H)	d(H···A)	d(D···A)	∠D−H···A
O10−H10···O3	0.86(3)	1.91(3)	2.697(6)	152(5)
O15−H15···O16	0.87(4)	1.83(3)	2.571(6)	142(5)
C13−H13B···O7	0.97	2.35	3.215(7)	149
C26−H26C···O2	0.96	2.31	2.976(8)	126
C28−H28B···O9	0.97	2.34	3.207(7)	148
C42−H42A···O2	0.96	2.34	2.991(9)	124
C43−H43C···O4	0.96	2.30	2.950(9)	125
C45−H45A···O4	0.96	2.37	3.006(9)	123

were C11–H11A···O1, C17−H17C···O1, respectively (Figure 4). In addition, there were four π − π interactions in the Cu (II) complex.[53,54]

3.3.2 | Crystal structure of the Co (II) complex

As shown in Figure 5, the Co (II) complex belongs to the monoclinic crystal system and the space group is $P\,2_1/n$.

The Co (II) complex was a dinuclear ($(L)^{2-}$:Co (II) = 2:2) structure, and both Co (II) atoms were pentacoordinated, forming triangular bipyramid geometries ($\tau_1 = 0.742$ and $\tau_2 = 0.648$). Take Co1 as an example, Co (II) atom was pentacoordinated with the two N atoms (N1 and N2) and two O atoms (O1 and O4) from the N_2O_2 cavity of the completely deprotonated ligand $(L)^{2-}$ unit, and one phenolic oxygen atom (O9) from the N_2O_2 cavity of another ligand $(L)^{2-}$ unit, the coordination distorted the two completely deprotonated ligand $(L)^{2-}$ units themselves to some extent. Comparing the Cu (II) complex with the Co (II) complex, it was found that the coordination of the Co (II) atoms with the phenoxy oxygen atoms of another ligand $(L)^{2-}$ unit was the main reason for the different configuration from the Cu (II) complex. Owing to the coordination of phenoxy oxygen atoms and the Co (II) atoms, the Co (II) complex had a completely different configuration from the Cu (II) complex.

The H atoms on the *tert-butyl* part of the completely deprotonated ligand $(L)^{2-}$ units and the phenoxy oxygen atoms on the neighboring deprotonated ligand $(L)^{2-}$ units formed intramolecular hydrogen bonds, C8–H8C···O1, C9–H9A···O1, C29–H29C···O6, and C30–H30A···O6, respectively. Other than that, there were two sets of intermolecular hydrogen bonds and a set of C–H···π interactions in the Co (II) complex, C21–H21B···O7, C42–H42C···O2, and C42−H42C···π, respectively (Figure 6).[55,56]

3.3.3 | Crystal structure of the Ni (II) complex

The crystal structure of the Ni (II) complex and the coordination configuration of Ni (II) atoms are shown in Figure 7. The Ni (II) complex was composed of two completely deprotonated ligand $(L)^{2-}$ units, three Ni (II) atoms, two bridging acetate groups, and two coordinated ethanol molecules as expected from the

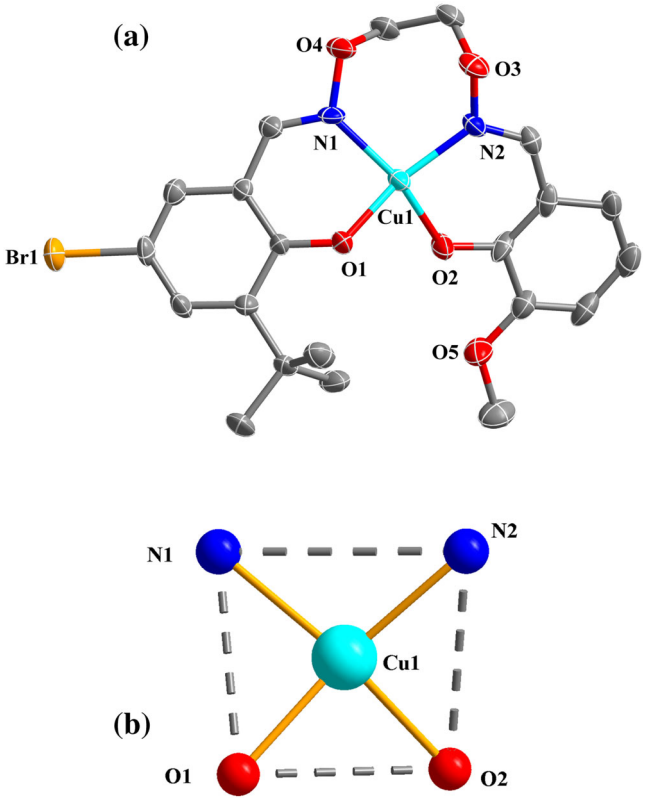

FIGURE 3 (a) The molecular structure of the Cu (II) complex (omitting hydrogen atoms for clarity). (b) Coordination polyhedron of Cu (II) atom of the Cu (II) complex

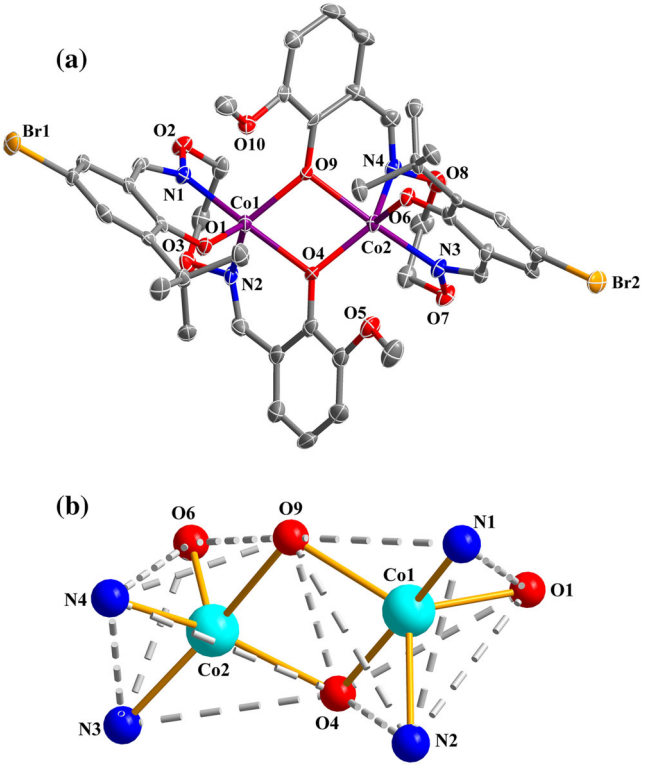

FIGURE 5 (a) The molecular structure of the Co (II) complex (omitting hydrogen atoms for clarity). (b) Coordination polyhedron of Co (II) atoms of the Co (II) complex

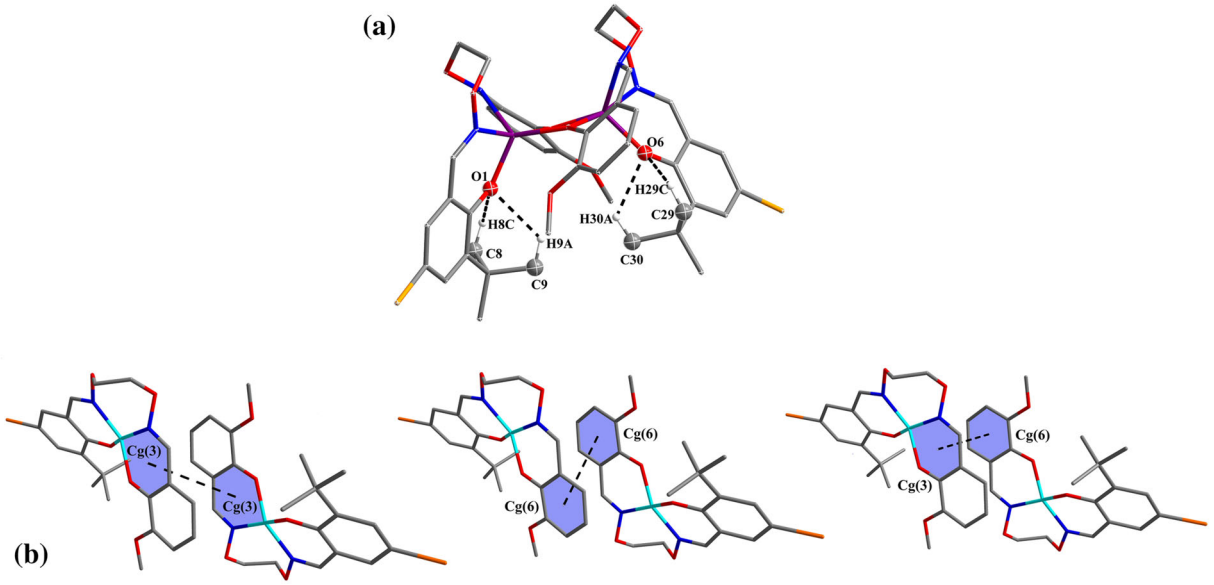

FIGURE 4 (a) The viewpoint of intramolecular hydrogen bonding interactions of the Cu (II) complex. (b) π···π stacking interactions of the Cu (II) complex

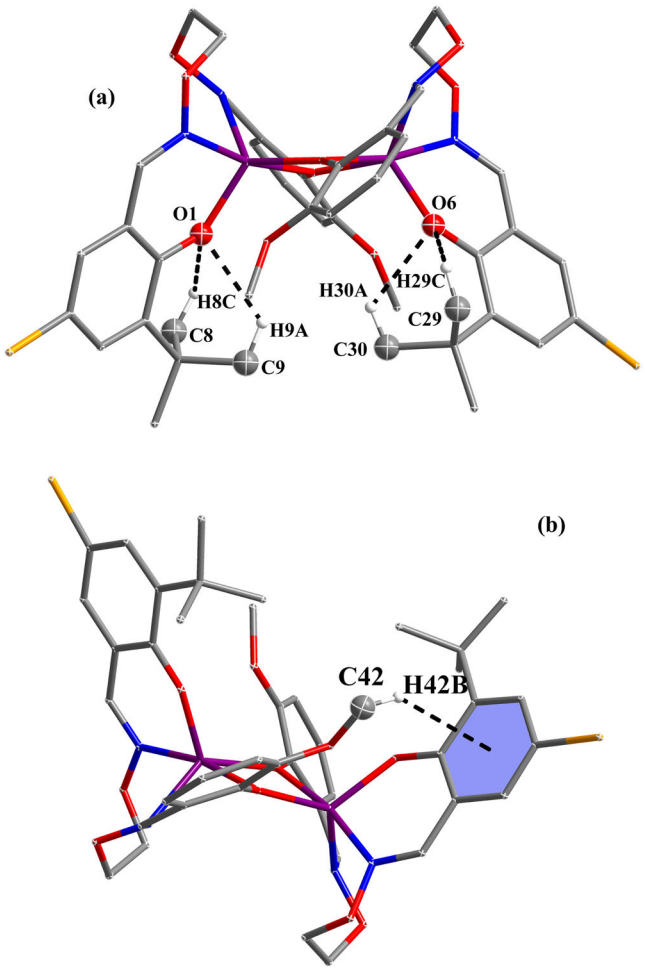

FIGURE 6 (a) The viewpoint of intramolecular hydrogen bonds of the Co (II) complex. (b) C–H···π stacking interactions of the Co (II) complex

elemental analytical data. The Ni (II) complex belongs to the monoclinic system and the space group is $P\ 2_1/n$.

The Ni (II) complex had a trinuclear structure, and all three Ni (II) atoms were hexacoordinated, forming octahedral geometries. The terminal Ni (II) atom (Ni1 or Ni2) was combined with two N atoms (N2, N3 or N1, N4) and two O atoms (O1, O2 or O4, O12) from the N_2O_2 cavity of the fully deprotonated ligand $(L)^{2-}$ unit, one O atom (O10 or O15) of the coordinated ethanol molecule and one O atom (O7 or O9) of the bridging acetate group. The central Ni (II) atom (Ni3) was composed of two μ-phenoxo oxygen atoms (O1 and O12) and two methoxy oxygen atoms (O5 and O11) from two [Ni(L)] chelates, and both oxygen atoms (O3 and O16) from the ligating acetate ions, μ O–C–O, also with octahedral geometry. The trinuclear structure was stabilized by two μ-acetate ligands which acted as a key role to connect Ni1 and Ni3 atoms (or Ni3 and Ni2). The main reason for the different configuration of the Ni (II) complex with the Cu (II) and Co (II) complexes was that the Ni (II) atoms were coordinated not only with μ-acetate ligands but also with methoxy oxygen atoms, finally, which formed a homotrinuclear ($(L)^{2-}$:Ni (II) = 2:3) complex, which was completely different from the coordination environments of the Cu (II) and Co (II) complexes.

There were eight groups of intramolecular hydrogen bonds in the Ni (II) complex, which are O10–H10···O3, O15–H15···O16, C13–H13B···O7, C26–H26C···O2, C28–H28B···O9, C42–H42A···O2, C43–H43C···O4, and C45–H45A···O4.[57,58] In addition, there were two groups of C–H···π and one group of C–Br···π interactions in the Ni (II) complex, which are C13–H13A···π, C26–H26A···π, and C18–Br1···π, respectively (Figure S4).

3.4 | Hirshfeld surfaces analyses

The three transition metal (II) complexes were investigated by Hirshfeld surfaces analyses using crystal Explorer software. Figure S5 showed the surface distribution of d_{norm} (standard high resolution) maps for the Cu (II), Co (II), and Ni (II) complexes. The red area represents the O–H interaction, and the deeper the red color, the stronger the O–H interaction.[59] The distribution of the interactions of C–H, Br–H, and H–H is mainly in the lighter color region. The distribution of hydrogen bond interactions can be roughly inferred from the diagram, which is helpful to further explore the internal factors of the stability of the complexes.[60]

In addition, the proportion of C–H/H–C, H–H, O–H/H–O, Br–H/H–Br interactions in the Cu (II), Co (II), and Ni (II) complexes can also be obtained by Hirshfeld surfaces analyses. The above short-range interactions were calculated theoretically, as shown in Figure S6. In the two-dimensional Hirshfeld surface generation diagram, the blue region represents the distribution of different short-range interactions, the upper left part represents the donor atom pointing to the receptor atom, and the lower right part is just opposite. For the Cu (II) complex, the ratios of C–H/H–C, H–H, O–H/H–O, Br–H/H–Br were 14.2%, 47.9%, 14.3%, and 11.5%, respectively. For the Co (II) complex, the proportions of C–H/H–C, H–H, O–H/H–O, Br–H/H–Br were 15.4%, 54.4%, 10.1%, and 14.5%, respectively. For the Ni (II) complex, the ratios of C–H/H–C, H–H, O–H/H–O, Br–H/H–Br were 8.2%, 68.1%, 5.3%, and 13.9% respectively. It was precisely because of these short-range interactions that the Cu (II), Co (II), and Ni (II) complexes are stable.

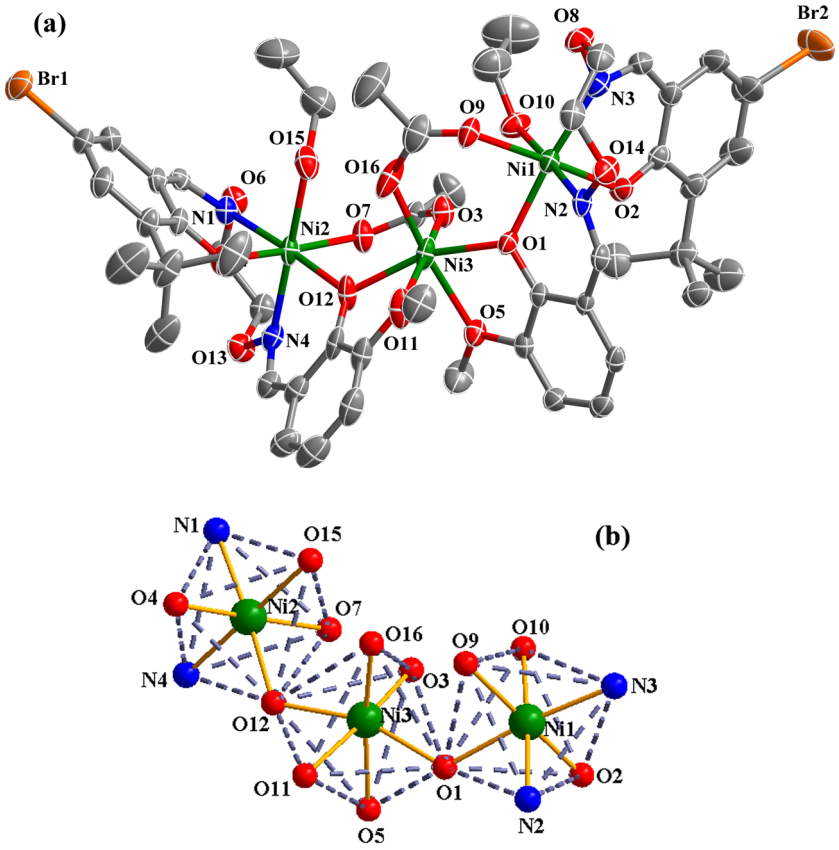

FIGURE 7 (a) The molecular structure of the Ni (II) complex (omitting hydrogen atoms for clarity). (b) Coordination polyhedrons of Ni (II) atoms of the Ni (II) complex

3.5 | Fluorescence properties

The fluorescence properties of the ligand H_2L and its Cu (II), Co (II), and Ni (II) complexes in DMF were tested at room temperature, as shown in Figure 8. At an excitation wavelength of approximately 276 nm, the ligand had a strong emission peak at approximately 389 nm, which was attributed to the $\pi - \pi^*$ transition.[2,8] The fluorescence of the Cu (II), Co (II), and Ni (II) complexes was all quenched, but the degree of quenching is different. The fluorescence quenching of the Cu (II) complex was the most serious, whereas the fluorescence quenching of the other Co (II) and Ni (II) complexes was less. The phenomenon of fluorescence quenching was due to LMCT caused by the coordination of the ligand H_2L with the Cu (II), Co (II), and Ni (II) atoms.[61]

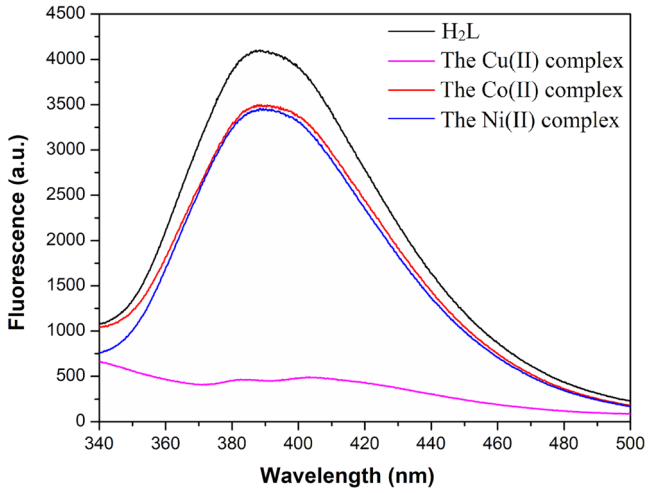

FIGURE 8 Fluorescence spectra of H_2L and its Cu (II), Co (II), and Ni (II) complexes

3.6 | Density functional theory calculation of the three metal complexes

The frontier orbit is the highest occupied molecular orbital (HOMO), and the lowest unoccupied molecular orbital (LUMO) is an important parameter of quantum chemistry.[62] The HOMO orbit is the electron-filled orbit with the highest energy, the least bound, and the most likely to lose electrons; the LUMO orbit is the unfilled electron orbit with the lowest energy, which is easy to accept electrons.[63] Therefore, the HOMO orbit determines the electronic gain and loss and transfer ability of molecules and determines the important chemical properties such as the orientation of intermolecular reactions.[64] The difference in energy and energy level is

important for studying the chemical properties of molecules.

For the α-spin orbit of the Cu (II) complex, the molecular orbital No.134 is the HOMO orbital, $E_{134} = -3.20927$ eV, the molecular orbital No.135 is the LUMO orbital, $E_{135} = -3.11375$ eV, and the energy gap $\Delta E = E_{135}\text{-}E_{134} = 0.00351$ eV. In order to fully analyze the charge density distribution, select the LUMO+2 (137), LUMO+1 (136), LUMO (135), HOMO (134), HOMO−1 (133), HOMO−2 (132) orbits to calculate the electron cloud and distribution (Figure S7a). It can be seen from the figure that the HOMO, LUMO of the α-spin orbit of the Cu (II) complex, and the electron clouds in the adjacent orbit mostly show local distribution. HOMO and LUMO orbital electron clouds were mainly distributed in the benzene ring part of 3-*tert-butyl*-5-bromosalicylic aldehyde, 6-methoxy-2-[*O*-(1-ethyloxyamide)]-oxime-1-phenol was on the benzene ring portion and Cu (II) atom. For the β-spin orbital of the Cu (II) complex, the molecular orbital No.133 is the HOMO orbital, $E_{133} = -4.03022$ eV, the molecular orbital No.134 is the LUMO orbital, $E_{134} = -3.20927$ eV, and the energy gap $\Delta E = E_{134}\text{–}E_{133} = 0.82096$ eV. In order to fully analyze the charge density distribution, choose to calculate the electron cloud and distribution of LUMO+2 (136), LUMO+1 (135), LUMO (134), HOMO (133), HOMO−1 (132), HOMO−2 (131) orbits, respectively (Figure S7b). It can be seen from the figure that the HOMO, LUMO of the β-spin orbit of the Cu (II) complex, and the electron clouds in the adjacent orbit mostly show local distribution. The HOMO electron cloud is mainly distributed on the benzene ring part of 3-*tert-butyl*-5-bromosalicylic aldehyde and the Cu (II) atom. LUMO electron cloud was mainly distributed in the benzene ring part of 3-*tert-butyl*-5-bromosalicylic aldehyde, 6-methoxy-2-[*O*-(1-ethyloxyamide)]-oxime-1-phenol is on the benzene ring portion and Cu (II) atom.

The calculation results of the Co (II) complex showed that the molecular orbital No.265 is a HOMO orbital, $E_{265} = 2.99076$ eV, the molecular orbital No.266 is a LUMO orbital, $E_{266} = 0.97878$ eV, and the energy gap $\Delta E = E_{266}\text{-}E_{265} = 3.96954$ eV, the energy gap is large. In order to fully analyze the charge density distribution, choose to calculate the electron cloud and distribution of LUMO+2 (263), LUMO+1 (264), LUMO (265), HOMO (266), HOMO−1 (267), and HOMO−2 (268) orbits, respectively (Figure S8). It can be seen from the figure that the HOMO, LUMO of the Co (II) complex, and the electron clouds in the adjacent orbits are mostly distributed locally. The HOMO and LUMO orbital electron clouds were mainly distributed on the benzene ring part of 6-methoxy-2-[*O*-(1-ethyloxyamide)]-oxime-1-phenol and two Co (II) atoms. There was no electron cloud distribution in the 3-*tert-butyl*-5-bromosalicylic aldehyde part, and the charge density was low.

The calculation results showed that for the α-spin orbit of the Ni (II) complex, the molecular orbital No.355 is the HOMO orbital, $E_{355} = -3.29035$ eV, the molecular orbital No.356 is the LUMO orbital, $E_{356} = -1.52545$ eV, the energy gap $\Delta E = E_{356}\text{–}E_{355} = 1.76490$ eV. In order to fully analyze the charge density distribution, choose to calculate the electron cloud and distribution of LUMO+2 (358), LUMO+1 (357), LUMO (356), HOMO (355), HOMO−1 (354), HOMO−2 (353) orbits respectively (Figure S9a). It can be seen from the figure that the HOMO, LUMO of the α-spin orbit of the Ni (II) complex, and the electron clouds in the adjacent orbits mostly show local distribution. HOMO and LUMO orbital electron clouds are mainly distributed on the benzene ring part and terminal Ni (II) atom of 3-*tert-butyl*-5-bromosalicylic aldehyde. For the β-spin orbital of the Ni (II) complex, the molecular orbital No. 354 is the HOMO orbital, $E_{354} = -3.26505$ eV, the molecular orbital No.355 is the LUMO orbital, $E_{355} = -1.20626$ eV, and the energy gap $\Delta E = E_{355}\text{–}E_{354} = 0.07566$ eV. In order to fully analyze the charge density distribution, select LUMO+2 (357), LUMO+1 (356), LUMO (355), HOMO (354), HOMO−1 (353), and HOMO−2 (352) orbits to calculate the electron cloud and distribution respectively (Figure S9b). It can be seen from the figure that the HOMO, LUMO of the β-spin orbit of the Ni (II) complex, and the electron clouds in the adjacent orbit mostly show local distribution. The HOMO electron cloud is mainly distributed on the benzene ring part of 3-*tert-butyl*-5-bromosalicylic aldehyde and the terminal Ni (II) atom. The LUMO electron cloud was mainly distributed on the benzene ring part of 6-methoxy-2-[*O*-(1-ethyloxyamide)]-oxime-1-phenol and the Ni (II) atoms at both ends.

3.7 | Antibacterial activities

Taking *E. coli* and *S. aureus* as antibacterial objects, the antibacterial activities of H_2L and the Cu (II), Co (II), and Ni (II) complexes were studied by Oxford cup method (Figure 9**)**. By measuring the diameter of inhibition zone, the antibacterial degree of H_2L and its Cu (II), Co (II), and Ni (II) complexes on *E. coli* and *S. aureus* was compared, as shown in Figure 10. Each complex was equipped with three gradient concentrations of solutions. DMF was used as a solvent for a blank experiment. Pour about 20 ml of culture medium into the sterilized plate, let it stand to coagulate horizontally, and inoculate 100 μl of bacterial solution and coat evenly. Next to the flame of the alcohol lamp, put a sterilized Oxford cup into the plate coated with bacterial solution, carefully draw 150 μl

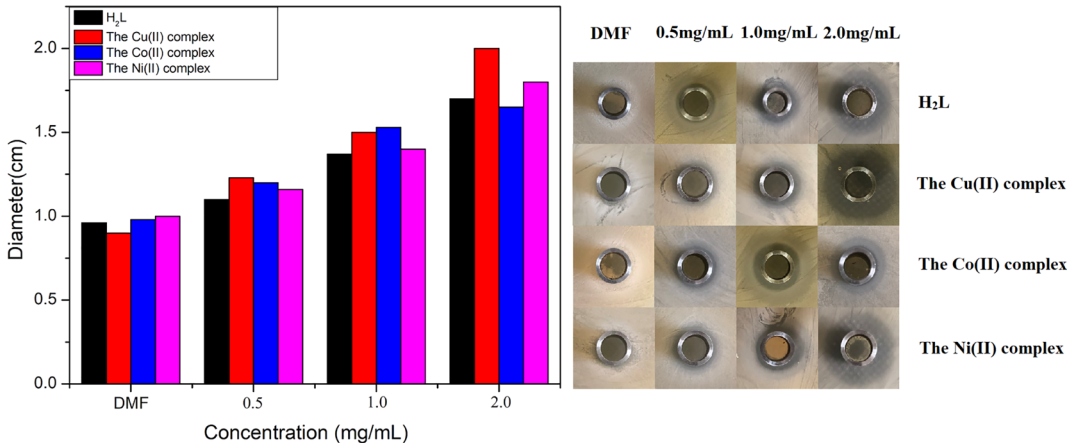

FIGURE 9 Histogram of the diameter of the bacteriostatic zone of *E. coli* in different concentration gradients of different samples and the diameter of *E. coli* bacteriostasis circle of different samples

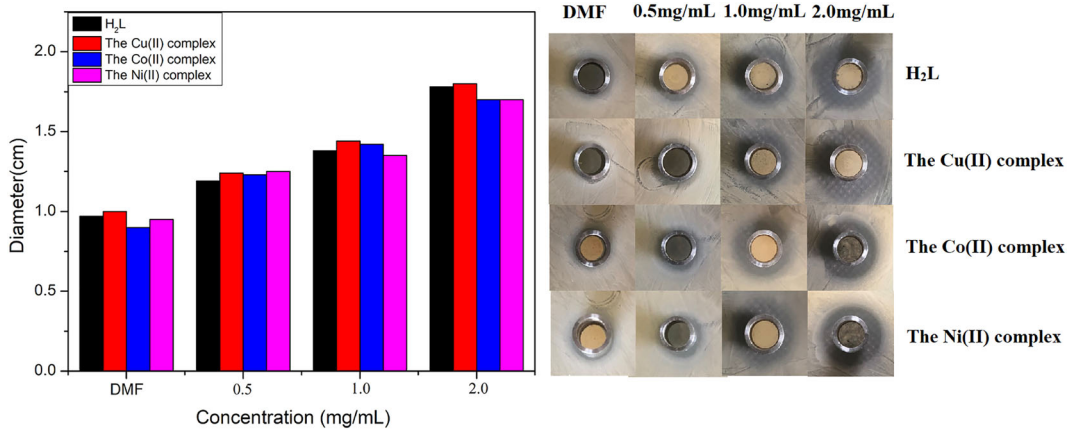

FIGURE 10 Histogram of the diameter of the bacteriostatic zone of *S. aureus* in different concentration gradients of different samples and the diameter of *S. aureus* bacteriostasis circle of different samples

of the prepared complex solution into the Oxford cup, cover the Petri dish cover, and incubate at 37°C cultivation in the box. After 24 h, take out and observe the antibacterial effect and take photos to record the size of the antibacterial circle.

It can be seen from the figure that the antibacterial effect of DMF is not obvious in the blank experiment. Both ligands and the Cu (II), Co (II), and Ni (II) complexes have bacteriostatic effects, but the degree of bacteriostasis varies. The inhibition diameters of the ligand H_2L as well as the three metal complexes were found to increase with increasing concentration against *E. coli* and *S. aureus*, with the Cu (II) complex possessing the best inhibition effect. This may be due to the direct interaction between the copper surface and the bacterial outer membrane, resulting in the rupture of the extracellular matrix. Then the copper surface acts on the holes in the bacterial outer membrane, causing the cells to lose the necessary nutrients and water, which eventually leads to atrophy.[65–67] The antibacterial activity of the Cu (II), Co (II), and Ni (II) complexes were similar, which were slightly stronger than that of the ligand and weaker than that of the Cu (II) complex.

4 | CONCLUSIONS

An asymmetric Salamo-based ligand H_2L was designed and synthesized. The three single crystals of the Cu (II), Co (II), and Ni (II) complexes derived from a ligand H_2L possessing three different coordination modes were obtained by natural volatile solvent method. The structures of the ligand H_2L and its Cu (II), Co (II), and Ni (II) complexes were determined by ^1H NMR and X-ray crystallographic analysis. The Cu (II) complex was formed by the coordination of the ligand $(L)^{2-}$ unit and one Cu (II) atom in the ratio of 1:1. The central Cu (II) atom was a tetracoordinated plane quadrilateral

geometry. The Co (II) complex was formed by the coordination of the two ligand $(L)^{2-}$ units and two Co (II) atoms in the ratio of 2:2. Both Co (II) atoms were all slightly distorted pentacoordinated triangular bipyramid geometries. The Ni (II) complex was composed of two completely deprotonated ligand $(L)^{2-}$ units, three Ni (II) atoms, two bridging acetate groups, and two coordinated ethanol molecules, and all the Ni (II) atoms were distorted hexacoordinated octahedral geometries. The density functional theory (DFT) was used to calculate the energy level of the corresponding orbit. Furthermore, the ligand H_2L and its Cu (II), Co (II), and Ni (II) complexes were also tested for antimicrobial activity. It was found that the ligand H_2L and its Cu (II), Co (II), and Ni (II) complexes inhibited *E. coli* and *S. aureus* to varying degrees.

ACKNOWLEDGEMENTS

This work was supported by the National Natural Science Foundation of China (21761018), Science and Technology Program of Gansu Province (18YF1GA057), and the Program for Excellent Team of Scientific Research in Lanzhou Jiaotong University (201706), three of which are gratefully acknowledged.

AUTHOR CONTRIBUTIONS

Ruo-Nan Bian: Data curation; formal analysis; investigation. **Ji-Fa Wang:** Data curation; investigation; methodology. **Xin Xu:** Data curation; formal analysis; investigation; methodology. **Xiu-Yan Dong:** Funding acquisition; project administration; resources. **Yu-Jie Ding:** Investigation; project administration.

CONFLICT OF INTEREST

The authors declare no competing financial interests.

DATA AVAILABILITY STATEMENT

The data that supports the findings of this study are available in the supporting information of this article.

REFERENCES

[1] J. Yu, Z. Zhu, Q. S. Ding, Y. Zhang, X. Y. Wu, L. Sun, J. Du, *Catal. Today* **2020**, *339*, 105.
[2] X. Xu, R. N. Bian, S. Z. Guo, W. K. Dong, Y. J. Ding, *Inorg. Chim. Acta* **2020**, *513*, 119945.
[3] P. Yadav, F. Zelder, *Chimia* **2020**, *74*, 252.
[4] C. Freire, M. Nunes, C. Pereira, D. M. Fernandes, A. F. Peixoto, M. Rocha, *Coordin. Chem. Rev.* **2019**, *394*, 104.
[5] A. Sumiyoshi, Y. Chiba, R. Matsuoka, T. Noda, T. Nabeshima, *Dalton Trans.* **2019**, *48*, 13169.
[6] H. R. Mu, M. Yu, L. Wang, Y. Zhang, Y. J. Ding, *Phosphorus, Sulfur Silicon Relat. Elem.* **2020**, *195*, 730.
[7] M. Saikawa, T. Noda, R. Matsuoka, T. Nakamura, T. Nabeshima, *Eur. J. Inorg. Chem.* **2019**, *6*, 766.
[8] R. N. Bian, J. F. Wang, Y. J. Li, Y. Zhang, W. K. Dong, *J. Photochem. Photobiol. A.* **2020**, *400*, 112719.
[9] T. Nakamura, Y. Kawashima, E. Nishibori, T. Nabeshima, *Inorg. Chem.* **2019**, *58*, 7863.
[10] L. W. Zhang, Y. Zhang, Y. F. Cui, M. Yu, W. K. Dong, *Inorg. Chim. Acta* **2020**, *506*, 119534.
[11] M. Yu, Y. Zhang, Y. Q. Pan, L. Wang, *Inorg. Chim. Acta* **2020**, *509*, 119701.
[12] S. Z. Zhang, J. Chang, H. J. Zhang, Y. X. Sun, Y. Wu, Y. B. Wang, *Chin. J. Inorg. Chem.* **2020**, *36*, 503.
[13] Y. Zhang, M. Yu, Y. Q. Pan, Y. Zhang, L. Xu, X. Y. Dong, *Appl. Organomet. Chem.* **2020**, *34*, e5442.
[14] C. Liu, X. X. An, Y. F. Cui, K. F. Xie, W. K. Dong, *Appl. Organomet. Chem.* **2020**, *34*, e5272.
[15] Y. Q. Pan, Y. Zhang, M. Yu, Y. Zhang, L. Wang, *Appl. Organomet. Chem.* **2020**, *34*, e5441.
[16] J. Chang, S. Z. Zhang, Y. Wu, H. J. Zhang, Y. X. Sun, *Transition Met. Chem.* **2020**, *45*, 101.
[17] Y. Q. Pan, X. Xu, Y. Zhang, Y. Zhang, W. K. Dong, *Spectrochim. Acta a* **2020**, *229*, 117927.
[18] L. Wang, Z. L. Wei, C. Liu, W. K. Dong, J. X. Ru, *Spectrochim. Acta a* **2020**, *239*, 118496.
[19] X. Liu, C. Manzur, N. Novoa, S. Celedónv, D. Carrillo, J. R. Hamonv, *Coordin. Chem. Rev.* **2018**, *357*, 144.
[20] R. Egekenze, Y. Gultneh, R. Butcher, *Polyhedron* **2018**, *144*, 198.
[21] V. Thamilarasan, P. Revathi, A. Praveena, J. Kim, V. Chandramohan, N. Sengottuvelan, *Inorg. Chim. Acta* **2020**, *508*, 119626.
[22] R. Mundil, J. Merna, Z. Hostalek, I. Sedenkova, *Macromol. Res.* **2015**, *23*, 161.
[23] C. C. Rocha, T. Onfroy, F. Launay, *C. R. Chim.* **2015**, *18*, 270.
[24] X. Y. Li, Q. P. Kang, C. Liu, Y. Zhang, W. K. Dong, *New J. Chem.* **2019**, *43*, 4605.
[25] L. Z. Liu, M. Yu, X. Y. Li, Q. P. Kang, W. K. Dong, *Chin. J. Inorg. Chem.* **2019**, *35*, 1283.
[26] M. Yu, H. R. Mu, L. Z. Liu, N. Li, Y. Bai, X. Y. Dong, *Chin. J. Inorg. Chem.* **2019**, *35*, 1109.
[27] L. Wang, Y. Q. Pan, J. F. Wang, Y. Zhang, Y. J. Ding, *J. Photochem. Photobiol. A.* **2020**, *400*, 112719.
[28] L. Wang, Z. L. Wei, Z. Z. Chen, C. Liu, W. K. Dong, Y. J. Ding, *Microchem. J.* **2020**, *155*, 104801.
[29] L. Z. Liu, L. Wang, M. Yu, Q. Zhao, Y. Zhang, Y. X. Sun, W. K. Dong, *Spectrochim. Acta a* **2019**, *222*, 117209.
[30] C. Liu, Z. L. Wei, H. R. Mu, W. K. Dong, Y. J. Ding, *J. Photochem. Photobio. A* **2020**, *397*, 112569.
[31] X. X. An, Z. Z. Chen, H. R. Mu, L. Zhao, *Inorg. Chim. Acta* **2020**, *511*, 119823.
[32] H. R. Mu, X. X. An, C. Liu, Y. Zhang, W. K. Dong, *J. Struct. Chem.* **2020**, *61*, 1218.
[33] O. V. Dolomanov, L. J. Bourhis, R. J. Gildea, J. A. K. Howard, H. J. Puschmann, *Appl. Cryst.* **2009**, *42*, 339.
[34] G. M. Sheldrick, *Acta Crystallogr., Sect. C: Cryst. Struct. Commun.* **2015**, *71*, 3.
[35] X. G. Guo, S. Qiu, X. T. Chen, Y. Gong, X. Q. Sun, *Inorg. Chem.* **2017**, *56*, 12357.
[36] Z. L. Wei, L. Wang, J. F. Wang, W. T. Guo, Y. Zhang, W. K. Dong, *Spectrochim. Acta a* **2020**, *228*, 117775.
[37] N. H. Yarkandi, H. A. El-Ghamry, M. Gaber, *Mat. Sci. Eng. C-Mater.* **2017**, *75*, 1059.

[38] M. Gaber, H. A. El-Ghamry, S. K. Fathalla, *Spectrochim. Acta a* **2015**, *139*, 396.
[39] X. X. An, Q. Zhao, H. R. Mu, W. K. Dong, *Crystals* **2019**, *9*, 101.
[40] Q. P. Kang, X. Y. Li, L. Wang, Y. Zhang, W. K. Dong, *Appl. Organomet. Chem.* **2019**, *33*, e5013.
[41] Q. P. Kang, X. Y. Li, Z. L. Wei, Y. Zhang, W. K. Dong, *Polyhedron* **2019**, *165*, 38.
[42] Q. Zhao, X. X. An, L. Z. Liu, W. K. Dong, *Inorg. Chim. Acta* **2019**, *490*, 6.
[43] Y. Zhang, L. Z. Liu, Y. D. Peng, N. Li, W. K. Dong, *Transition Met. Chem.* **2019**, *44*, 627.
[44] H. S. Tahereh, K. Alireza, S. Esmail, J. Jan, *Inorg. Chim. Acta* **2020**, *506*, 119537.
[45] P. Sen, D. Akagunduz, A. S. Aghdam, F. C. Cebeci, T. Nyokong, T. Catal, *J. Inorg. Organomet. Polym. Mater.* **2019**, *30*, 1110.
[46] A. A. Elif, E. Gökçe, Ö. Namık, S. E. Kuruca, B. D. Tülay, *New J. Chem.* **2020**, *44*, 5333.
[47] Y. Onami, T. Kawasaki, H. Aizawa, T. Haraguchi, T. Akitsu, K. Tsukiyama, M. A. Palafox, *Int. J. Mol. Sci.* **2020**, *21*, 874.
[48] Q. Wu, J. D. Li, F. X. Liu, J. C. Xiao, Y. F. Tang, Q. L. Zi, *Russ. J. Coord. Chem.* **2020**, *46*, 137.
[49] S. Prasenjit, G. Samir, C. P. Ganesh, K. Mahmuda, B. Surajit, M. Chandan, *Inorg. Chim. Acta* **2020**, *502*, 119340.
[50] H. Oshita, T. Suzuki, K. Kawashima, H. Abe, F. Tani, S. Mori, T. Yajima, Y. Shimazaki, *Dalton Trans.* **2019**, *48*, 12060.
[51] M. Azam, S. I. A. Resayes, T. K. Agata, R. Kruszynski, S. F. Adil, N. K. Lokanath, J. Saudi, *Chem. Soc.* **2019**, *23*, 636.
[52] H. Oshita, T. Suzuki, K. Kawashima, H. Abe, F. Tani, S. Mori, T. Yajima, Y. Shimazaki, *Chem. – Eur. J.* **2019**, *25*, 7649.
[53] Z. L. Wei, L. Wang, S. Z. Guo, Y. Zhang, W. K. Dong, *RSC Adv.* **2019**, *9*, 41298.
[54] L. Wang, Z. L. Wei, M. Yu, Y. Q. Pan, Y. Zhang, W. K. Dong, *Chin. J. Inorg. Chem.* **2019**, *35*, 1791.
[55] X. X. An, C. Liu, Z. Z. Chen, K. F. Xie, W. K. Dong, *Crystals* **2019**, *9*, 602.
[56] Y. F. Cui, Y. Zhang, K. F. Xie, W. K. Dong, *Crystals* **2019**, *9*, 596.
[57] Y. Zhang, Y. Q. Pan, M. Yu, X. Xu, W. K. Dong, *Appl. Organomet. Chem.* **2019**, *33*, e5240.
[58] L. Xu, M. Yu, L. H. Li, J. C. Ma, W. K. Dong, *J. Struct. Chem.* **2019**, *60*, 1358.
[59] D. Milenković, E. Avdović, D. Dimić, S. Sudha, D. Ramarajan, Z. Milanović, S. Trifunović, Z. S. Marković, *J. Mol. Struct.* **2020**, *1209*, 127935.
[60] A. Laachir, S. Guesmi, E. M. Ketatni, M. Saadi, L. E. Ammari, S. Esserti, M. Faize, F. Bentiss, *J. Mol. Struct.* **2020**, *1218*, 128533.
[61] Y. X. Sun, Y. Q. Pan, X. Xu, Y. Zhang, *Crystals* **2019**, *9*, 607.
[62] T. A. Yousef, *J. Mol. Struct.* **2020**, *1215*, 128180.
[63] S. Saouli, I. Selatnia, B. Zouchoune, A. Sid, S. M. Zendaoui, C. Bensouici, E. E. Bendeif, *J. Mol. Struct.* **2020**, *1213*, 128203.
[64] R. Kaliammal, S. Sudhahar, G. Parvathy, K. Velsankar, K. Sankaranarayanan, *J. Mol. Struct.* **2020**, *1212*, 128069.
[65] V. T. Nguyen, K. S. Trinh, *Braz. J. Chem. Eng.* **2019**, *36*, 1553.
[66] K. M. Takroni, H. A. El-Ghamry, A. Fawzy, *J. Inorg. Organomet. Polym. Mater.* **2020**, *29*, 1927.
[67] M. Gaber, H. A. El-Ghamry, S. K. Fathalla, M. A. Mansour, *Mat. Sci. Eng. C-Mater.* **2018**, *83*, 78.

SUPPORTING INFORMATION

Additional supporting information may be found online in the Supporting Information section at the end of this article.

How to cite this article: Bian R-N, Wang J-F, Xu X, Dong X-Y, Ding Y-J. Investigation of mononuclear, dinuclear, and trinuclear transition metal (II) complexes derived from an asymmetric Salamo-based ligand possessing three different coordination modes. *Appl Organomet Chem*. 2020; e6040. https://doi.org/10.1002/aoc.6040